Analysis of Permanent Magnet Synchronous Motors with Integer-slot and Fractional-slot Windings

J. A. Güemes[#1], A. M. Iraolagoitia[#2], M. P. Donsión[*3], P. Fernández[+4]

[#] *Department of Electrical Engineering, E. U. de Ingenieria Técnica Industrial, University of the Basque Country*
Plaza de la Casilla 3, 48012 Bilbao, Spain
[1] joseantonio.guemes@ehu.es
[2] ana.iraolagoitia@ehu.es

[*] *Department of Electrical Engineering, University of Vigo*
Campus of Lagoas Marcosende, 36310 Vigo (Spain)
[3] donsion@uvigo.es

[+] *Department of Electronics and Telecommunications, E.U. de Ingenieria Técnica Industrial, University of the Basque Country*
Plaza de la Casilla 3, 48012 Bilbao, Spain
[4] pablo.fernandezr@ehu.es

***Abstract*— This paper examines torque ripple, cogging torque, and d-axis and q-axis reactances variation in permanent magnet synchronous motors (PMSMs). Effect of number of poles on electromagnetic motor torque (including cogging torque), and d- and q-axis reactance, has been analyzed for two different PMSM configurations having the same envelop dimensions and output requirements. Finite element technique is used for computation of the machine characteristics. Maxwell stress tensor is used to find the torque.**

I. INTRODUCTION

PMSM are widely used in many industrial applications for their high efficiency, compact structure, high torque-to-current and torque-to-volume ratios, fast dynamic response, simple mechanical construction, absence of moving contact and easy maintenance. As their cost continues to decrease they have the opportunity to become a dominant force in the industrial applications market [1] - [3].

One of the most important problems in permanent magnet motors is the torque ripple which is inherent in their design. This ripple is parasitic, and can lead to mechanical vibration, acoustic noise, and problems in drive systems. Minimizing this ripple is of great importance in the design of PMSMs. Pulsating torque should be specially analyzed for the application of constant speed or high-precision position control, especially at low speed [1]-[2], [4]-[5].

There are three sources of torque ripple coming from the machine: a) cogging torque, b) difference between permeances of the air gap in the *d*- and *q*-axis (reluctance torque), and c) distortion of the magnetic flux density waveform in the air gap [6]. Cogging torque is the consequence of interaction (magnetic attraction) between rotor-mounted permanent magnets field and the stator teeth, which produces reluctance variations depending on rotor position; it is independent of stator current. It manifests itself by the tendency of the rotor to align in a number of stable positions even when machine is unexcited, resulting in a pulsating torque which does not contribute to the net effective torque of the motor.

In the literature, numerous methods for reducing the cogging torque, such as employing a fractional number of slots per pole, skewing of magnets or stator lamination stack (slots), displacing and shaping the magnets, optimizing the magnet pole-arc-to-pole-pitch ratio, introducing auxiliary slots or teeth, etc, have been proposed [3]-[4], [7]-[12], However, optimizing the cogging torque to a low value is not sufficient to obtain a low torque ripple [3], [10], [13]. As a consequence, in motor design process, the problem of the torque ripple reduction should be considered as a whole.

Minimizing torque ripple is of utmost importance in many industrial applications and this is the reason it has received much attention in recent years. Different techniques for torque ripple minimization have been proposed in literature. Broadly speaking, these techniques can be divided into two main groups.

The first class concentrates on the optimum motor design subject to the constraints of minimum pulsating torque and maximum average torque. Several torque ripple minimization techniques for surface-mounted magnet motors have been proposed [3], [10], [14]-[15]. Use of the same approach for interior-mounted magnet motors is troublesome and imprecise, and is almost absent in literature.

The second class is based on the drive and control concept to generate an appropriate control effort to minimize the torque ripple [16]-[20].

In PMSM, apart from estimating torque ripple, is also important to calculate equivalent circuit parameters of the motor. Knowledge of the different parameters of the equivalent circuit allows us to know the behaviour of the machine, by applying the laws of electrical circuits.

It is well known that the *d*- and *q*-axis reactances are the most significant parameters when dealing with steady state and/or dynamic performance analysis of PMSMs. These

978-1-4244-5794-6/10/$26.00 ©2010 IEEE

reactances are also very important for designing control systems, in order to maximize the efficiency, power factor, etc.

In the literature, various techniques have been described to predict the *d*- and *q*-axis inductances [21]-[26].

The main objective of this paper is to investigate the influence of pole number on the torque ripple (including cogging torque) and *d*- and *q*-reactances of two 36-slot three-phase PMSMs with the same envelop dimensions and output requirements. Magnetic vector potential waveforms in the air gap are also obtained and compared.

Finite element technique is used for the computation of the machine characteristics. Core saturation is directly considered in the magnetic field calculation. Maxwell stress method is used to find the torque. The *d*- and *q*-reactances determination is carried out through input energy calculation of the 2D model (effects such as stator end-winding leakage and magnet skew can be easily included using classical formulas). Implementation can be conveniently realized by using commercially available and technically mature finite element packages.

II. Analyzed Motors

Cross section of two 36-slot PMSMs, discussed in this paper, is shown in Fig. 1. Each rotor pole contains a permanent magnet of the neodymium-iron-boron type (NdFeB) that is magnetized across their shorter dimension along the d-axis.

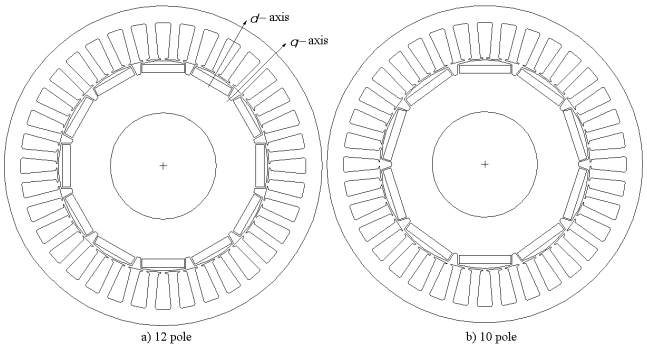

Fig. 1. Cross section of the motors

Table I shows the main design parameters of the studied motors.

TABLE I
DETAILS OF THE ANALYZED MOTORS

Connection	Star
Power rating	6 kW
Number of poles	12 – 10
Frequency of the motor input voltage	19.2 – 16 Hz
Number of stator slots	36
Rotor outside diameter	158 mm
Stator inner diameter	160 mm
Stator outside diameter	240 mm
Magnet thickness	6 mm
Width of magnet	32 – 39 mm
Magnet pole-arc-to-pole-pitch ratio	0,79 - 0.81
Coercive magnetizing intensity	920 kA/m
Remanent flux density	1.16 T

III. Model and Method

Finite element technique is used for machine characteristics computation. Finite element models are two-dimensional plane. A non-lineal field analysis is carried out for calculating the magnetic vector potential and magnetic flux density in each node of the finite element model. Stator winding is excited with three-phase balanced sinusoidal currents to produce the characteristic synchronously rotating magnetomotive force waveform.

The model is constituted by a transverse section through the middle of the motor (360º geometry). The space of air surrounding the motor has to be taken into account too.

Figure 2 shows the finite element mesh used.

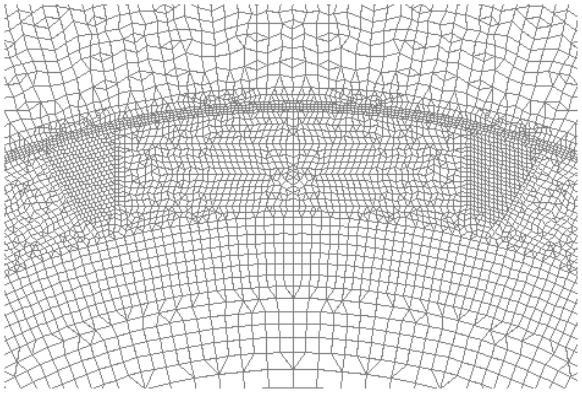

Fig. 2. Two-dimensional meshing model (zoom)

Torque is calculated using the Maxwell stress method [27]-[29]. This method requires the local flux density distribution along a specific line or contour.

Total force can be calculated by means of the following expression:

$$\boldsymbol{F} = \int_s \frac{1}{2\mu_o}\left(B_n^2 - B_t^2\right) ds \cdot \boldsymbol{n} + \int_s \frac{1}{\mu_o} B_n B_t ds\, \boldsymbol{t} \qquad (1)$$

where B_n and B_t, are the normal and tangential components of the magnetic flux density, $\boldsymbol{n}$ and $\boldsymbol{t}$ are the normal and tangential unit vectors to the surface of integration *s*.

Taking into account that in rotating electric machine only the tangential component of the Maxwell stresses generates torque, we have:

$$\boldsymbol{F}_t = \int_s \frac{1}{\mu_o} B_n B_t ds \qquad (2)$$

For two-dimensional plane models the integration surface is transformed into a closed contour of radius *r* (air gap region centre). Calculating the tangential force in each point of the round path, by means of the following expression:

$$F_t = \frac{B_n\, B_t}{\mu_o} d\, l \qquad (3)$$

where *d* is the length of the path between two consecutive nodes and *l* is the axial length of the magnetic sheet core.

As the magnetic flux density is calculated at discrete points in the air gap region, the torque can be obtained by means of the following expression:

$$T = r\left(\sum \frac{l}{\mu_o} B_n\, B_t\, d\right) l \qquad (4)$$

where r is the radius of the circular path taken.

Torque calculation by means of (4) depends strongly on the path and mesh structure and a considerable care is required with mesh discretization in the air gap in order to achieve high accuracy. To minimize errors integration contour was established in the middle of air gap with a four-layer mesh (see Fig. 2).

IV. Torque

Variations in cogging torque, average torque and torque ripple for two motor configurations indicated above are analyzed in this section.

A. Cogging torque

The combinations of pole and slot number of a motor have influence on frequency and peak value of cogging torque waveform.

Cogging torque is the oscillatory torque consequence of interaction between rotor-mounted permanent magnets field and the stator teeth, which produces reluctance variations depending on rotor position. Cogging torque exists even when there is no stator current.

The smallest common multiple (*LCM*) of stator slot number (K) and pole number ($2p$) represents number of cogging torque cycles per mechanical revolution (n_r), thus cycle number per slot pitch (n_p) is the ratio between *LCM* and *K:*

$$n_p = \frac{LCM(K,2p)}{K} \qquad (5)$$

If division between stator slot number and pole number is an integer, only one cogging torque cycle per slot appears and so, cycle number per mechanical revolution is the same than slot number.

n_p should be as high as possible since a higher period number of cogging torque results in a smaller peak value. Generally, a high n_p value also has a mitigating effect on the current-dependent ripple torque.

Another index for checking the level of cogging torque is the greatest common divisor (*GCD*) of K and $2p$. Structural periodicity exists around the air gap every 360/(GCD) mechanical degrees. The smaller *GCD(K,2p)* is, smaller will be cogging torque.

Table II shows number of slots (K), number of poles ($2p$), number of slots per pole and phase (q), winding factor (k_w), slot pitch (p_s), pole pitch (p_p), least common multiple between the pole number and the stator slot number *LCM*(K,$2p$), number of periods of the cogging torque waveform per slot pitch (n_p) and greatest common divisor between slot number and pole number *GCD*(K,$2p$) for two different PMSM configurations analyzed in this paper.

TABLE II
PARAMETERS OF ANALYZED MOTORS

K	$2p$	p_s	q	k_w	p_p	LCM	n_p	GCD
36	12	10º	1	1	30º	36	1	12
36	10	10º	1.2	0.956	36º	180	5	2

To calculate cogging torque, behaviour of the motor for different rotor positions (when there is no current in the windings) is simulated; at each rotor position the meshing is renewed.

Figure 3 shows the cogging torque as a function of mechanical angle for the two different motors configurations.

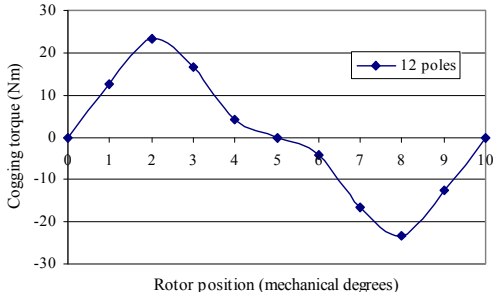

a) 12 pole motor

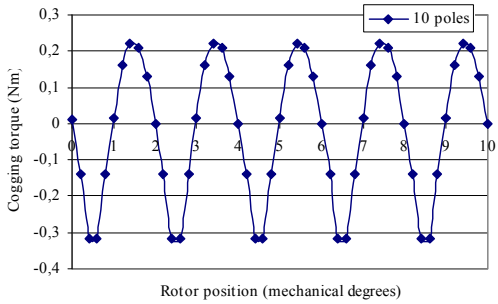

b) 10 pole motor

Fig. 3. Cogging torque in a slot pitch

Table III shows peak-to-peak value of the cogging torque (T_{cpp}), in two analyzed motors.

TABLE III
PEAK-TO-PEAK VALUE OF COGGING TORQUE

Motor	**T_{cpp} (Nm)**
12 pole	46
10 pole	0.53

From the results, it can be seen that: a) the two motor configurations have the same slot pitch (10 mechanical degrees), but differ in cogging-torque waveform periods number (five in 10 pole motor and one in 12 pole motor), and b) the peak-to-peak value of the cogging torque is reduced by 98.8 % for 10 pole motor compared to the peak-to-peak value obtained with the 12 pole motor.

B. Torque ripple

Electromagnetic torque developed by the motor is calculated simulating load behaviour of the motor, for different positions of the rotor, when armature flux linkage and excitation are perpendicular ($I_d = 0$, $I_q = I$).

Figure 4 shows the torque ripple as a function of mechanical angle for the two analyzed motors. It is clear that the pulsating torque period is 12 mechanical degrees in 10 pole motor, and 10 degrees in 12 pole motor (both cases 3 cycles per pole pitch), and the torque ripple is smaller in fractional winding motor than in integer winding motor.

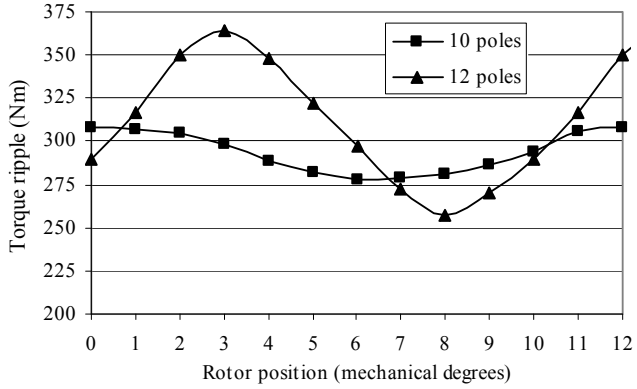

Fig. 4. Torque ripple

Torque ripple factor (t_r) can been defined as following [6]:

$$t_r = \frac{T_{max} - T_{min}}{T_{av}} \cdot 100 \tag{6}$$

where T_{max},, T_{min} and T_{av} are respectively, maximum, minimum and average values of the torque.

Cogging torque factor (t_c) can be defined as follows:

$$t_r = \frac{T_{cpp}}{T_{av}} \cdot 100 \tag{7}$$

Table IV shows maximum, minimum, average values of the torque (T_{max}, T_{min} and T_{av}, respectively), torque ripple factor (t_r), peak-to-peak value of the cogging torque (T_{cpp}) and cogging torque factor (t_c) for the two analyzed motor configurations.

TABLE IV
TORQUE RIPPLE FACTOR AND COGGING TORQUE FACTOR

Motor	T_{max} (Nm)	T_{min} (Nm)	T_{av} (Nm)	t_r (%)	T_{cpp} (Nm)	t_c (%)
12 pole	364	258	308	34.4	46	15
10 pole	307	278	293	9.9	0.53	0.18

We can observe that 10 pole motor average developed torque (293 Nm) is 4.9% lower than 12 pole motor average torque (308 Nm), and magnitude of the torque ripple factor is reduced by 72 % for 10 pole motor compared to 12 pole motor.

Based on the result shown above, the 10 pole motor with a fractional-slot winding and a high number of cogging torque cycles per mechanical revolution, have a lower torque ripple that the 12 pole motor. However 10 pole motor has a low GDC which points out radial magnetic-force unbalance, vibration and magnetic noise [30]. Depending on the specific application and operating requirements of the motor, this effect should be studied.

V. DIRECT AND QUADRATURE REACTANCES

Electrical machines are usually represented, in electrical engineering, by means of their equivalent circuit. The knowledge of the different parameters of the equivalent circuit allows us to know the behaviour of the machine, by applying the laws of electrical circuits. The circuit equivalent parameters of a PMSM are the resistance and the *d*- and *q*-axis reactances.

Estimation of the machine phase resistance at room temperature is relatively easy and there is no need to estimate it by FEM.

For PMSM with surface mounted magnets, the *d*- and *q*-axis reactances are approximately equal (the modern permanent magnets have relative permeability close to unity, therefore the effective air gap seen from the stator is nearly independent of the position). For salient pole permanent magnet motors X_q is larger than X_d since the flux path passes through a magnet (which have a relative permeability close to unity) in the *d*-axis, but through magnetic iron in the *q*-axis.

The *d*-and *q*-axis inductance, L_d and L_q, respectively, can be calculated as follows [6]-[18]:

$$L_d = \frac{\Psi_d - \Psi_m}{I_d}; \quad L_q = \frac{\Psi_q}{I_q} \tag{8}$$

where Ψ_d and Ψ_q are the total fluxes in the *d*-axis and *q*-axis, I_d and I_q are the *d*-axis and *q*-axis armature currents, and Ψ_m is the flux-linkage due to the permanent magnets.

The whole procedure to calculate the *d*-axis and *q*-axis reactances may be described in terms of the following sequence of steps:

(a) to calculate the *d*-axis and *q*-axis inductance, L_d^{2D} and L_q^{2D}, respectively, by simulating the magnetic performance of the motor without considering the 3D effects;
(b) to calculate the end-winding leakage inductance;
(c) to determine the *d*-axis and *q*-axis inductance, L_d and L_q, respectively, by adding the inductances calculated in the steps (a) and (b).

By using the finite element method and by means of two behaviour analysis of the motor, the *d*-axis inductance can be calculated. In a first analysis the no-load behaviour of the motor is simulated. In a second analysis the load behaviour of the motor when the armature flux and the excitation flux are in the same direction ($I_d = I$; $I_q = 0$) is simulated.

The *q*-axis inductance can be calculated, by simulating the load behaviour of the motor when the armature flux is perpendicular to excitation flux ($I_d = 0$; $I_q = I$)

The end-winding inductance can be calculated from [31], as follows:

$$L_{ew} = 8\pi 10^{-7}\, p\, q^2\, Z_n^2 \left(0.67 l_{ew} - 0.43 y_c \tau_s\right) \tag{9}$$

where Z_n is the number of conductors per slot, l_{ew} is the average length of end-winding, y_c is the coil pitch in slot pitches and τ_s is the slot pith.

The resultant *d*- and *q*-axis inductances can be calculated by means of the following expressions:

$$L_d = L_d^{2D} + L_{ew} \;;\; L_q = L_q^{2D} + L_{ew} \tag{10}$$

Finally, the *d*- and *q*-axis reactances can be calculated as follows:

$$X_d = 2\pi f L_d \quad ; \quad X_q = 2\pi f L_q \tag{11}$$

where *f* is the supply frequency.

Table V shows the reactances' values obtained for two analyzed motors.

TABLE V
REACTANCES

Motor	X_d (Ω)	X_q (Ω)
12 pole	5.1	7.1
10 pole	5.9	7.5

VI. MAGNETIC VECTOR POTENTIAL AND MAGNETIC FLUX DENSITY

Figures 5 to 7 show the air-gap magnetic vector potential waveforms obtained, once the no-load and load analysis of the motors have been carried out. In this figures, the horizontal axis represents the position of an observer inside the air gap of the machine. The origin of coordinates corresponds, in both motors, to the beginning of a polar pitch. The peak value of the magnetic vector potential on no-load by the 10 pole motor is 25.9 % higher compared to magnetic vector potential on no-load by 12 pole motor (see Fig. 5). The use of fractional number of slots per pole increases the fundamental order (deformation of the magnetic-vector-potential waveform in the air gap of the machine), since the stator slots are located at different relative circumferential positions with respect to the edges of the magnets (see Fig. 6 and 7).

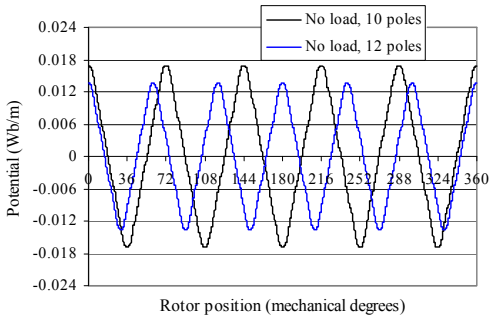

Fig. 5. Magnetic vector potential in no-load text

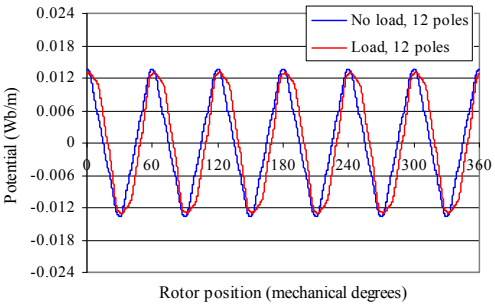

Fig. 6. Magnetic vector potential in 12 pole motor

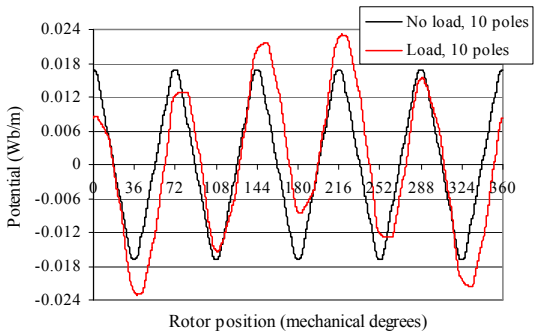

Fig. 7. Magnetic vector potential in 10 pole motor

Figures 8 to 10 show the normal component of the magnetic flux density in the centre of air gap versus rotor position for the two motor configurations investigated. We can see that magnetic flux density in no-load condition by 10 pole motor is 4.5 % higher compared to 12 pole motor (see Fig. 8).

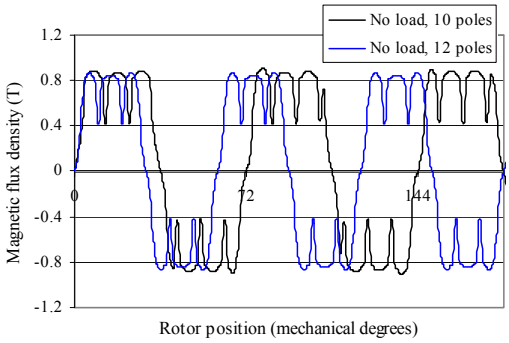

Fig. 8. Component normal of flux density (no-load test)

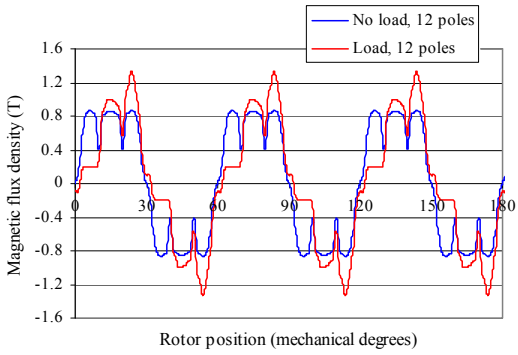

Fig. 9. Component normal of flux density in 12 pole motor

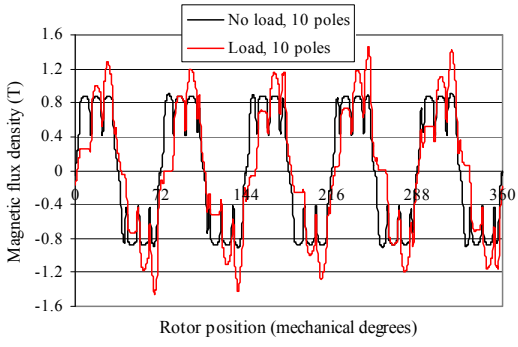

Fig. 10. Component normal of flux density in 10 pole motor

VII. CONCLUSIONS

The effect of the pole number on torque ripple (including the cogging torque) has been investigated for two different PMSM configurations having the same envelop dimension and output requirements. The motor with fractional-slot winding have a lower cogging torque and torque ripple but show a reduction of the average torque.

The period number by pole pitch of the torque ripple waveform is the same in both motors.

The 10 pole motor has a magnetic flux density in no-load condition higher that 12 pole motor however, the average torque is lower.

The magnetic-flux-density normal component and magnetic vector potential distribution along the air gap by two PMSM configurations have been investigated. Assuming a pure sinusoidal phase current distribution, the use of fractional number of slots per pole, increases harmonics' content of the magnetic vector potential and normal component of the magnetic flux density waveforms.

REFERENCES

[1] L. Dosiek, and P. Pillay, "Cogging torque reduction in permanent magnet machines", *IEEE Trans. Industry Application,* Vol. 43, No. 6, pp. 1656–157, 2007.

[2] L. Wu, W. Jin, J. Ni, and J. Ying, "A Cogging torque reduction method for surface mounted permanent magnet motor", in *Proc. International Conference on Electrical Machines and Systems*, Seoul – Korea, 2007, pp. 769–773.

[3] R. Islam, I. Husain, A. Fardoun, and K. McLaughlin, "Permanet-magnet synchronous motor magnet designs with skewing for torque ripple and cogging torque reduction", *IEEE Trans. Industry Applications,* Vol. 45, No. 1, pp. 152-160, 2009.

[4] Z.Q. Zhu, and D. Howe, "Influence of design parameters on cogging torque in permanent magnet machines", *IEEE Trans. Energy Conversion*, Vol. 15, No. 4, pp. 407-412, 2000.

[5] R. Lateb, N. Takorabet, and F. Meibody-Tabar, "Effect of magnet segmentation on the cogging torque in surface-mounted permanent-magnet motors", *IEEE Trans. Magnetics*, Vol. 42, No. 3, pp. 442-445, 2006.

[6] J. F. Gieras, and M. Wing, *Permanent magnet motor technology. Design and Applications*, Marcel Dekker**,** 2002.

[7] T. Li, and G. Slemon, "Reduction of cogging torque in PM motors", *IEEE Trans. Magnetics,* Vol. 24, No. 6, pp. 2901–2903, 1988.

[8] T. Ishikawa, and G. R. Slemon, "A method of reducing ripple torque in permanent magnet motors without skewing", *IEEE Trans. Magnetics,* Vol. 29, No. 2, pp. 2028-2031, 1993.

[9] E. R. Braga, and A. M. N. Lima, "Reducing cogging torque in interior permanent magnet machines without skewing", *IEEE Tran. Magnetics,* Vol. 34, No. 5, pp. 3562–3565, 1998.

[10] P. Salminen, J. Pyrhönen, F. Libert, and J. Soulard, "Torque ripple of permanent magnet machines with concentrated windings", in *Proc. International Symposium on Electromagnetic Fields in Mechatronics, Electrical and Electronic Engineering*, Baiona - Spain, Sep. 2005.

[11] Z..Q. Zhu, S. Ruangsinchaiwanich, and D. Howe, "Synthesis of cogging-torque waveform form analysis of a single stator slot", *IEEE Trans. Industry Applications*, Vol. 42, No. 3, pp. 650-657, 2006.

[12] C. Schlensok, M. Herranz-Gracia, and K. Hameyer, "Combined numerical and analytical method for geometry optimization of a PM motor", *IEEE Trans. Magnetics*, vol. 42, no. 4, pp. 1211-1214, 2006.

[13] J. A. Güemes, A. M. Iraolagoitia, M. P. Donsión, and J. I. Del Hoyo, "Analysis of torque in permanent magnet synchronous motors with fractional slot windings", in *Proc. International Conference on Electrical Machines*, Vilamora – Portugal, 2008.

[14] C. A. Borghi, D. Casadei, A. Cristofolini, and G. Serra, "Application of a multiobjective minimization technique for reducing the torque ripple in permanet-magnet motors," IEEE Trans. Magnetics, vol. 35, pp. 4238-4246, Sept. 1999.

[15] C. A. Borghi, D. Casadei, A. Cristofolini, M. Fabbri, and G. Serra, "Minimizing torque ripple in permanent magnet synchonous motors with polymer-bounded magnet," IEEE Trans. Magnetics, vol. 38, pp. 1371- 1377, Mar. 2002.

[16] W. Qian, S. K. Panda, and J. X. Xu, "Torque ripple minimization in PM synchronous motors using iterative learning control," *IEEE Trans. Power electronics*, vol. 19, pp. 272-279, Mar. 2004.

[17] [17] V. Petrović, R. Ortega, A. M. Stanković, and Tandmor, "Design and implementation of an adaptive controller for torque ripple minimization in PM synchonous," IEEE Trans. Power Electronics, vol. 15, pp. 871-879, Sept. 2000.

[18] J. X. Xu, S. K. Panda, Y. J. Pan, T. H. Lee, and B. H. Lam, "A modular control scheme for PMSM speed control with pulsating torque minimization," IEEE Trans. Industrial Electronics, vol. 51, pp. 526-536, June 2004.

[19] P. Mattavelli, L. Tubiana, and M. Zigliotto, "Torque-ripple reduction in PM synchronous motor drives using repetitive current control," IEEE Trans. Power Electronics, vol. 20, pp. 1423-1431, Nov. 2005.

[20] Y. Abdel-Rady, I. Mohamed, and E. F. El-Saadany, "A current control scheme with an adaptive internal model for torque ripple minimization and robust current regulation in PMSM drive systems," IEEE Trans. Energy conversion, vol. 23, pp. 92-100, Mar. 2008.

[21] D. Pavlik, V. K. Garg, J. R. Repp and J. Weiss, "A finite element technique for calculating the magnet sizes and inductances of permanent magnet machines", *IEEE Trans. Energy Conversion*, Vol. 3, No. 1, pp. 116-122, 1988.

[22] L. Chang, "An Improved FE inductance calculation for electrical machines", *IEEE Trans. Magnetics*, Vol. 32, No. 4, pp. 3237-3245, 1996.

[23] H. P. Nee, L. Lefevre, P. Thelin and J. Soulard, "Determination of *d* and *q* reactances of permanent-magnet synchronous motors without measurements of the rotor position", *IEEE Trans. Industry Applications*, Vol. 36, No. 5, pp. 1330-1335, 2000.

[24] E. C. Lovelace, T. M. Jahns and J. H. Lang, "A saturating lumpend-parameter model for an interior PM synchronous machine", *IEEE Trans. Industry Applications,* Vol, 38, No. 3, pp. 645-650, 2002.

[25] Y. S. Chen, Z.Q. Zhu and D. Howe, "Calculation of d- and q-axis inductances of PM brushless ac machines accounting for skew", *IEEE Trans. Magnetics*, Vol. 41, No. 10, pp. 3940-3942, 2005.

[26] K. M. Rahman, and S. Hiti, "Identification of machine parameters of a synchronous motor", *IEEE Trans. Industry Applications*, Vol. 41, No. 2, pp. 557-565, 2005.

[27] S. Salon, S. Bhatia, and D. Burow, "Some aspects of torque calculations in electrical machines", *IEEE Trans. Magnetics*, Vol. 33, No, 2, pp. 2018-2021, 1997.

[28] J. Mizia, K. Adamiak, A. R., Eastham, and G. E. Dawson, "Finite element force calculation: comparison of methods for electric machines", *IEEE Trans. Magnetics*, Vo. 24, No. 1, pp. 447-450, 1988.

[29] W. Zhu, S. Pekarek, B. Fahimi, and B. J. Deken, "Investigation of force generation in a permanent magnet synchronous machine", *IEEE Trans Energy Conversion*, Vol. 22, No. 3, pp. 557-565, 2007.

[30] F. Magnussen, and H. Lendenmann, "Parasitic effects in PM machines with concentrated windings", *IEEE transactions on industry applications*, vol. 43, No. 5, pp. 1223-1232, Sep./Oct. 2007.

[31] J. Corrales, *Cálculo industrial de máquinas eléctricas*. Tomo I, Marcombo Bouxareu Editores, Barcelona- Spain, 1982.